Journal of Solid State Chemistry 183 (2010) 408–418

Contents lists available at ScienceDirect

Journal of Solid State Chemistry

journal homepage: www.elsevier.com/locate/jssc

$LiZnNb_4O_{11.5}$: A novel oxygen deficient compound in the Nb-rich part of the Li_2O–ZnO–Nb_2O_5 system

Vladimir A. Morozov [a,*], Alla V. Arakcheeva [b,c], Vera V. Konovalova [d], Philip Pattison [b,e], Gervais Chapuis [b], Oleg I. Lebedev [f], Valery V. Fomichev [d], Gustaaf Van Tendeloo [f]

[a] Chemistry Department, Moscow State University, 119991 Moscow, Russia
[b] Ecole Polytechnique Fédérale de Lausanne, Laboratoire de Cristallographie, BSP, CH-1015 Lausanne, Switzerland
[c] Baykov Institute of Metallurgy and Material Sciences RAS, Leninsky pr., 49, 119991 Moscow, Russia
[d] Material Science and New Materials Department, Moscow State Academy of Fine Chemical Technology, 119571 Moscow, Russia
[e] Swiss–Norwegian Beamline, ESRF, BP-220, F-38043 Grenoble CEDEX, France
[f] EMAT, University of Antwerp, Groenenborgerlaan 171, B-2020, Antwerp, Belgium

ARTICLE INFO

Article history:
Received 29 October 2009
Received in revised form
3 December 2009
Accepted 8 December 2009
Available online 16 December 2009

Keywords:
Complex niobium oxides
α-PbO_2 related structure
Superspace approach
Supercell
(3+1)D structure type
X-ray diffraction
Transmission electron microscopy

ABSTRACT

A novel lithium zinc niobium oxide $LiZnNb_4O_{11.5}$ (LZNO) has been found in the Nb-rich part of Li_2O–ZnO–Nb_2O_5 system. LZNO, with an original α-PbO_2 related structure, has been synthesized by the routine ceramic technique and characterized by X-ray diffraction and transmission electron microscopy (TEM). Reflections belonging to the LZNO phase, observed in X-ray powder diffraction (XRPD) and electron diffraction, have been indexed as monoclinic with unit cell parameters a=17.8358(9) Å, b=15.2924(7) Å, c=5.0363(3) Å and γ=96.607(5)° or as α-PbO_2-like with lattice constants a=4.72420(3) Å, b=5.72780(3) Å, c=5.03320(3) Å, γ=90.048(16)° and modulation vector $\mathbf{q}=0.3\boldsymbol{a}^*+1.1\boldsymbol{b}^*$ indicating a commensurately modulated α-PbO_2 related structure. The monoclinic cell is a supercell related to the latter. Using synchrotron powder diffraction data, the structure has been solved and refined as a commensurate modulation (superspace group $P112_1/n(\alpha\beta0)00$) as well as a supercell (space group $P2_1/b$). The superspace description allows us to consider the LZNO structure as a member of the proposed α-PbO_2-Z (3+1)D structure type, which unifies both incommensurately and commensurately modulated structures. HRTEM reveals several types of defects in LZNO and structural models for these defects are proposed. Two new phases in Li_2O–ZnO–Nb_2O_5 system are predicted on the basis of this detailed HRTEM analysis.

1. Introduction

Lithium niobate (LN: $LiNbO_3$) is an important material in the optical industry and it is of great interest for many applications, such as optical waveguides, surface acoustic wave devices, electro-optic modulators, second harmonic generators, holographic storage and others [1]. Li-deficiency in LN crystals introduces intrinsic defects [2] which significantly increase the photorefractive effect and thus reduce the optical damage resistance. These defects can be reduced by increasing the stoichiometry or adding some dopants [3]. Usually, commercial LN crystals for laser applications are doped with MgO for increasing the damage threshold [4]. However, a different type of optical damage (the so-call dark trace) induced by a high-power laser beam still remained in the MgO-doped crystals. This limits their performance in high-power applications. Volk et al. [5] reported that the dark trace could be removed by using ZnO-doping. An optimization of the photorefractive and optical properties of ZnO-doped LN crystals requires a detailed knowledge of the phase formation in the Li_2O–ZnO–Nb_2O_5 system especially in the Nb-rich part.

Two lithium zinc niobium oxides $LiZnNbO_4$ [6] and $Li_{2.98}Zn_{0.51}Nb_2O_7$ [7] are known in the Li_2O–ZnO–Nb_2O_5 system. The first one crystallizes in the spinel-type structure while the structure of the second compound is unknown. The phase formation in the ZnO–Nb_2O_5 system however is better studied in the Zn-rich part; the ZnO–Nb_2O_5 phase diagram shows two congruent compounds having compositions $Zn_3Nb_2O_8$ ($3ZnO{:}Nb_2O_5$) and $ZnNb_2O_6$ ($ZnO{:}Nb_2O_5$) [8]. Later Ballman and Brown showed that $ZnNb_2O_6$ is not congruently melting [9]. $ZnNb_2O_6$ forms in a columbite-type (or α-PbO_2-type) structure [10] in direct equilibrium with β-Nb_2O_5 and not as a low temperature transformation from the rutile structure [9,11]. $Zn_7Nb_2O_{12}$ ($7ZnO{:}Nb_2O_5$) with a cubic spinel structure is formed in the presence of ZnO vapour [12]. The $Zn_4Nb_2O_9$ ($4ZnO{:}Nb_2O_5$) phase with a corundum-related structure has been prepared at

* Corresponding author. Fax: +7 495 939 33 16.
E-mail address: morozov@tech.chem.msu.ru (V.A. Morozov).

0022-4596/$ - see front matter © 2009 Elsevier Inc. All rights reserved.
doi:10.1016/j.jssc.2009.12.008

1973 K, using a pressure of P=9 GPa [13]. $Zn_{0.67}Nb_{11.33}O_{29}$ ($2ZnO{:}17Nb_2O_5$) crystallizes in monoclinic and orthorhombic modifications and is found in the Nb-rich part of the ZnO–Nb_2O_5 phase diagram [14]. In addition to LN ($Li_2O{:}Nb_2O_5$) only the $LiNb_3O_8$ ($Li_2O{:}3Nb_2O_5$) phase is known in the Nb-rich part of the Li_2O–Nb_2O_5 system [15,16].

In this paper, we study a novel compound, $LiZnNb_4O_{11.5}$, in the Nb-rich part of the Li_2O–ZnO–Nb_2O_5 system and discuss the relation of the $LiZnNb_4O_{11.5}$ structure with the structure of α-PbO_2 [17].

2. Experimental

Lithium zinc niobium oxide $LiZnNb_4O_{11.5}$ (LZNO) is synthesized from a (1:2:4) stoichiometric mixture of Li_2CO_3 (99.99%), ZnO (99.99%) and Nb_2O_5 (99.99%) by the routine ceramic technique at 1323 K for 100 h in air followed by quickly quenching from 1323 K to liquid nitrogen. XRD pattern of $LiZnNb_4O_{11.5}$ has been checked using the JCPDS PDF-2 Data Base and does not contain reflections of initial phases and previously known $LiNb_3O_8$ or $ZnNb_2O_6$ phases (Cards 36-0307 and 37–1371).

Lithium, zinc and niobium contents were determined by inductively coupled plasma (ICP) emission spectrometry performed on a JY-38P (Jobin Yvon, France) equipped with a monochromator with linear dispersion 0.56 nm mm^{-1}, RF plasma generator with power output of 1.5 kW at 27.12 MHz and photoelectric registration of the spectrum radiation intensity. For ICP measurements the LZNO sample has been fused with $K_2S_2O_7$ (99.99%) at 1023 K for 100 h in a quartz crucible. After cooling, the melt was immersed in a pyrex beaker containing a 2 M H_2SO_4 (concentrated) and 5% H_2O_2 (70% solution) mixture and heated on a hot plate at 353 K for 2 h till complete sample dissolving. For determination of Li, Zn and Nb the prepared initial solution has been diluted by distilled water to 5 times, 20 times and 200 times, respectively.

Second-harmonic generation (SHG) responses of the powder samples were measured in reflection mode. A Q-switch pulsed Nd:YAG laser operated at a wavelength of λ_ω=1064 nm was used as a radiation source with a repetition rate of 4 pulses per second and a pulse duration of about 12 ns. The laser beam was split into two beams to excite the radiation at the halve wavelength, $\lambda_{2\omega}$=532 nm, simultaneously on samples to be measured and on a reference sample: polycrystalline α-SiO_2. The incident-beam peak power was about 0.1 MW on a spot of 3 mm in diameter on the surface of the sample. The absence of a noticeable SHG signal confirms the choice of a centrosymmetric space group.

Thermogravimetric (TG) and differential scanning calorimetric (DSC) measurements for LZNO were performed on a NETZSCH STA 409 thermoanalyzer in the temperature range from 300 to 1323 K with heating/cooling rates of 10 K/min. Sintered kaolin was used as reference material. Weigh loss or the absence of some thermal effects were not observed on heating/cooling TG and DSC curves, respectively. TG and DSC measurements show that LZNO is stable in the temperature range from 300 to 1323 K without any first order phase transition in the structure.

X-ray powder diffraction (XRPD) data were collected at room temperature on a SIEMENS D500 diffractometer equipped with a primary SiO_2 monochromator (Cu$K\alpha_1$ radiation, λ=1.5406 Å, Bregg–Brentano geometry) and a position sensitive detector (BRAUN). The data were collected over the range of 5°–100° in 2θ° with steps of 0.02 °2θ.

X-ray synchrotron powder diffraction data were collected at the beamline BM01A (Swiss-Norwegian Beamline) at ESRF, Grenoble. A wavelength of 0.6942 Å was selected using a Si(111) double crystal monochromator, and the synchrotron beam was focused to a size of 0.3 mm × 0.3 mm using a combination of curved mirrors and a sagitally bent second crystal. The sample was positioned into a borosilicate capillary of 0.5 mm diameter, and the data were collected at room temperature. A mar345 image plate detector was used to register the powder patterns. The sample-to-detector distance of 250 mm was calibrated using a LaB_6 reference powder. Exposure time was typically 30 s per image, and the sample was rotated during the data collection at a speed of 1 degree per second. Exposure times were chosen to avoid any pixel saturation. The integration of the 2D powder data was done using the fit2d software package [18]. The powder diffraction data cover the range $0.0025 \le 2\theta \le 34.758$ with steps of 0.005 °2θ. Rietveld [19] refinements of LZNO structure were carried out using the JANA2006 [20] programme packages. Illustrations were produced with the JANA2006 programme packages in combination with the program DIAMOND [20].

Electron diffraction (ED) and high-resolution transmission electron-microscopy (HRTEM) investigations were made on crushed samples deposited on holey carbon grids. Energy dispersion X-ray (EDX) analysis and ED patterns were obtained using a Philips CM20 microscope with a LINK-2000 attachment. For the EDX analysis, results were based on the Nb_L and Zn_L lines in the spectra. HRTEM observations were performed using a JEOL 4000 EX microscope operating at 400 kV having 1.7 Å point resolution. Simulations of the HREM images were performed using the CrystalKit and MacTempas software packages.

3. Results

3.1. Elemental contents

The elemental analysis performed by ICP gives for the Li, Zn and Nb content 1.2+0.2, 10.7+0.5, and 59.0%+1.8 wt%, respectively. This is close to the $LiZnNb_4O_{11.5}$ composition (calc. wt%: 1.11 (Li), 10.42 (Zn), 59.18 (Nb) and 29.30 (O)).

The Zn:Nb ratio was confirmed by local EDX analysis in the transmission electron microscope, in combination with ED for structure identification of each crystallite. The cation ratio was found to be Zn:Nb=1.0:4.00 (19.5 ± 2.0 at% Zn, 80.5 ± 2.0 at% Nb). This is close to the bulk LZNO composition determined by ICP and reveals a homogenous element distribution in the sample.

3.2. X-ray powder diffraction

A preliminary analysis of strong reflections in the XRPD pattern revealed the new compound to have α-PbO_2 related substructure (space group *Pbcn*) with unit cell parameters: a=4.727 Å, b=5.731 Å, c=5.0363 Å, V=136.4 Å^3. However, several extra reflections were visible in the pattern (Fig. 1), which could not be assigned to any previously known $LiNb_3O_8$ or $ZnNb_2O_6$ phase. The reflections belonging to the LZNO phase qwere indexed on the base of a monoclinic unit cell with unique c axis: (1) a=18.5788(9) Å, b=15.2924(7) Å, c=5.0363(3) Å and γ=107.517(5)° or (2) a=17.8358(9) Å, b=15.2924(7) Å, c=5.0363(3) Å and γ=96.607(5)°. According to one of the standard crystallography rules, if a crystal structure can be described in two or more different monoclinic settings (space group, unit cell parameters, etc.), the setting with the minimal deviation of the monoclinic angle from 90° should be selected. Systematic extinctions (0k0, k=2n; 00l, l=2n; hk0, k=2n) together with the SHG data result in the space group $P2_1/b$.[1]

[1] The transformation matrix from the orthorhombic α-PbO_2 subcell to the monoclinic LZNO supercell is $T=\begin{pmatrix}1 & \bar{3} & 0\\ 3 & 1 & 0\\ 0 & 0 & 1\end{pmatrix}$ in the matrix equation $A_{LZNO}=A_{\alpha\text{-}PbO2}T$.

The ratio between the volume of the LZNO supercell (S.G. $P2_1/b$: a=17.8358(9) Å, b=15.2924(7) Å, c=5.0363(3) Å, γ=96.607(5)°, V=1364.5 Å^3) and the α-PbO_2 substructure is close to 10. Lead and oxygen atoms in the α-PbO_2 substructure (Z=4) occupy the 4-*fold* (symmetry 4*c*) and 8-*fold* (symmetry *8d*) positions, respectively. The atom coordinates for the $P2_1/b$ supercell model of LZNO structure have been obtained by transforming the coordinates of the corresponding positions in the α-PbO_2 substructure in accordance with the transformation matrix. As a result of the transformation, cations and oxygen atoms in the $P2_1/b$ monoclinic supercell occupy 10 and 20 (4-*fold*) positions, respectively. According to the ICP data (Li:Zn:Nb=1:1:4) 40 cation sites are occupied by $6\frac{2}{3}Li^+$, $6\frac{2}{3}Zn^{2+}$ and $26\frac{2}{3}Nb^{5+}$ while $76\frac{2}{3}$ oxygen atoms occupy 80 sites. Thus LZNO has an oxygen deficient α-PbO_2 related structure with a random distribution of lithium, zinc and niobium at the cation sites of the structure.

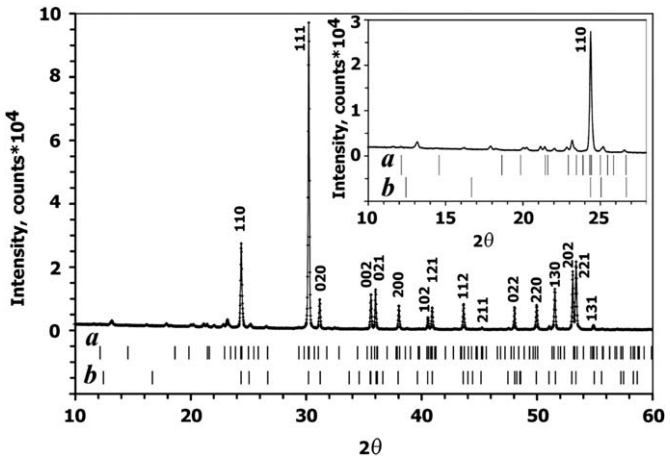

Fig. 1. Experimental XRD patterns for $LiZnNb_4O_{11.5}$. Tick marks denote the peak positions of possible Bragg reflections for $LiNb_3O_8$ (a) and $ZnNb_2O_6$ (b) phases. The inset shows a part of the profile in the low angle region. The *hkl* indexation of strong reflections is given for α-PbO_2 substructure (space group *Pbcn*).

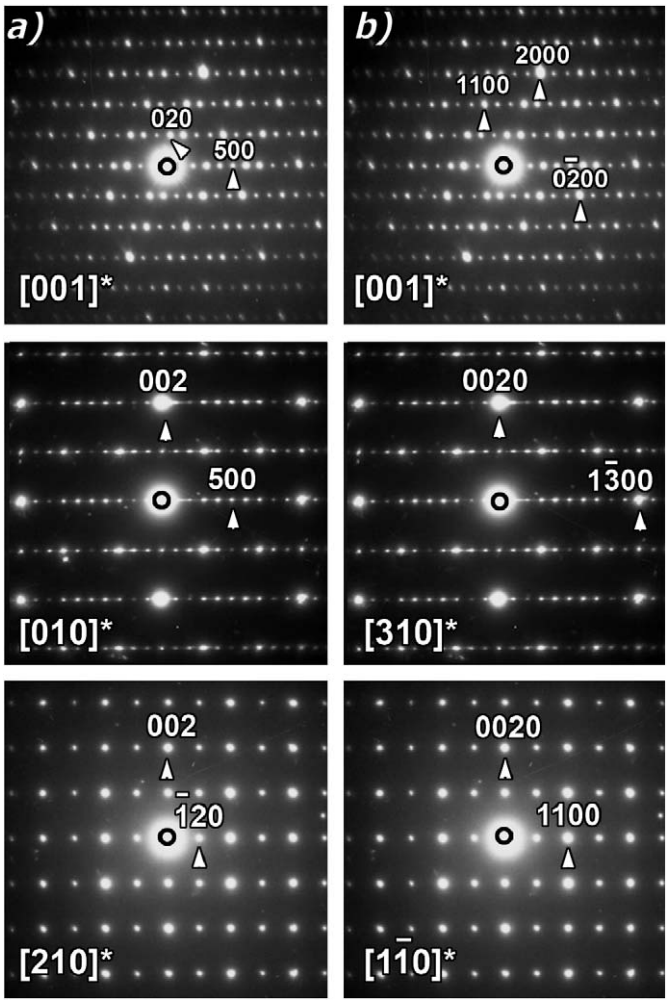

Fig. 2. Electron diffraction patterns along the main zone axes for $LiZnNb_4O_{11.5}$: (a) indexing in the $P2_1/b$ monoclinic unit cell; (b) indexing in the superspace group $P112_1/n(\alpha\beta 0)00$.

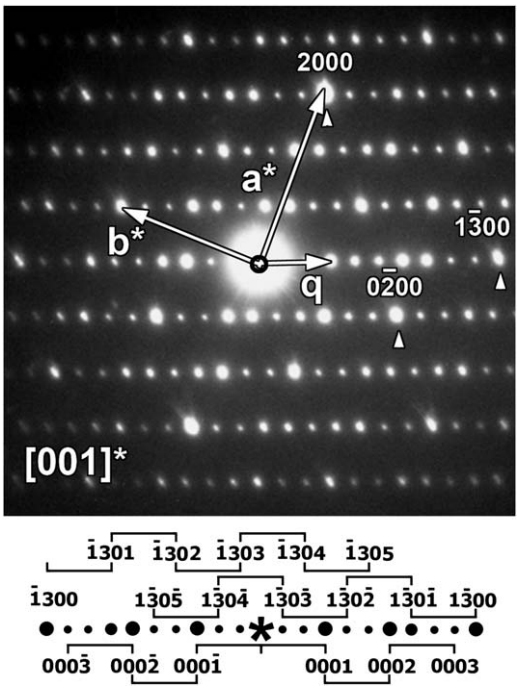

Fig. 3. Indexation scheme of the [001]* ED pattern of the commensurate modulated $LiZnNb_4O_{11.5}$ phase.

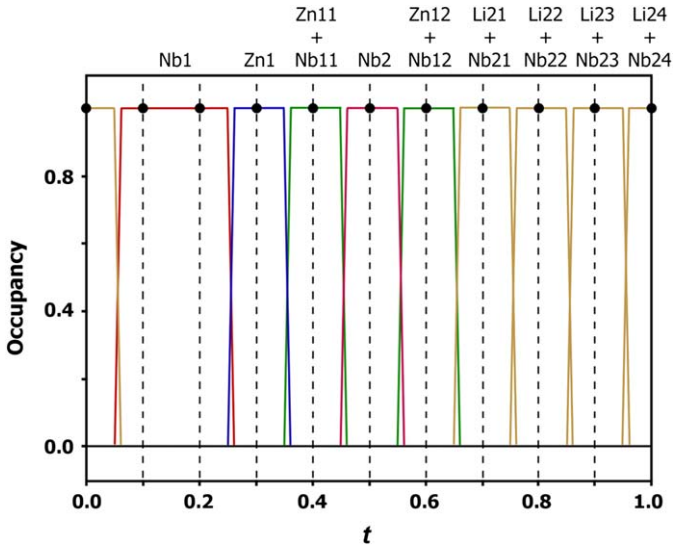

Fig. 4. (Colour online). Scheme of the crenel occupation modulation function of the Li, Zn and Nb distribution in the cation position as a function of *t*. Only 10 (black) points corresponding to intersections of the function with dashed lines refer to the commensurately modulated structure of $LiZnNb_4O_{11.5}$.

3.3. Electron diffraction

The reconstruction of reciprocal space, carried out by tilting around the major crystallographic axes, allowed the determination of the cell parameters and the conditions limiting the reflections (Fig. 2). ED patterns for LZNO along the main zone axes are shown in Fig. 2a. All reflections in the [010]*, [210]* and [001]* ED patterns can be completely indexed in a *P*-monoclinic unit cell in accordance with the unit cell parameters determined from XRPD data (Fig. 2a). The [010]* and [210]* ED patterns exhibit 00*l* reflections with *l*-odd. However, these reflections disappear when the crystallite is tilted around the [00*l*]* row, i.e., when double diffraction conditions are avoided. The presence of these 00*l* reflections with *l*-odd is therefore attributed to double diffraction and only 0*l*0 reflections with $l=2n$ are allowed.

On the other hand, all reflections in ED patterns for LZNO can also be indexed in a modulated α-PbO_2 related structure with unit cell parameters $a=4.727$ Å, $b=5.731$ Å, $c=5.0363$ Å, $\gamma\approx 90^\circ$ and a modulation vector $\mathbf{q}=0.3\mathbf{a}^*-0.9\mathbf{b}^*$, which implies a commensurate modulation (Fig. 2b). The modulation lowers the three-dimensional symmetry from *Pbcn* to $P112_1/n$, which together with the **q** vector suggests the superspace group $P112_1/n(\alpha\beta0)00$. The ED patterns can be completely indexed with four *hklm* indexes given by the diffraction vector $\mathbf{g}=h\mathbf{a}^*+k\mathbf{b}^*+l\mathbf{c}^*+m\mathbf{q}$, where

Table 2
Positions and compositions of atomic domains represented by the crenel occupation modulation function obtained from the refinement of the commensurately modulated $LiZnNb_4O_{11.5}$ structure ((3+1)D group $P112_1/n(\alpha\beta0)00$, $a=4.72420(3)$ Å, $b=5.72780(3)$ Å, $c=5.03320(3)$ Å, $\gamma=90.048(16)^\circ$, $q=0.3a^*+1.1b^*$).

Atomic domain	Δ[a]	o[a]	Composition
*M*11=Zn11+Nb11	0.1	0.15	0.33(1)Zn+0.67(1)Nb
*M*12=Zn12+Nb12	0.1	0.35	0.33(1)Zn+0.67(1)Nb
*M*21=Li21+Nb21	0.1	0.45	0.17Li+0.83(2)Nb
*M*22=Li22+Nb22	0.1	0.55	0.72Li+0.28(2)Nb
*M*23=Li23+Nb23	0.1	0.65	0.28Li+0.72(1)Nb
*M*24=Li24+Nb24	0.1	0.75	0.50Li+0.50(1)Nb
Nb1	0.2	0.90	1.0Nb
Nb2	0.1	0.25	1.0Nb
Zn1	0.1	0.05	1.0Zn

[a] Δ and o refer the length and the center of a domain within a single translation along the x_4 axis.

Table 1
Details of the $LiZnNb_4O_{11.5}$ structure refinement using both superspace and supercell models.

	Superspace model	Supercell model
Chemical formula	$LiZnNb_4O_{11.5}$	$LiZnNb_4O_{11.5}$
Formula weight	418.8	418.8
Temperature (K)	293	293
Cell setting	Monoclinic	Monoclinic
(Super) Space group	$P2_1/n(\alpha\beta0)00$	$P2_1/b$
Lattice parameters:		
a (Å)	4.72420(3)	17.8243(2)
b (Å)	5.72780(3)	15.2854(3)
c (Å)	5.03320(3)	5.03377(5)
γ (°)	90.048(16)	96.6139(16)
V (Å^3)	136.195(2)	1362.33(4)
q vector	$0.3a^*+1.1b^*$	
Formula units, Z	0.667	6.667
Calculated density, D_x (g cm^{-3})	5.1041	5.1026
Color	White	White
Data collection		
Diffractometer	MAR345	
Radiation type/wavelength (λ) (Å)	Synchrotron/0.6942 Å	
Radiation monochromator	Si(111) double crystal	
2θ range (°)	0.0025–34.758	
Step scan (2θ)	0.005	
I_{max}	52491	
Number of points	6950	
Refinement		
Refinement	Rietveld	Rietveld
Background function	Legendre polynomials, 17 terms	Legendre polynomials, 17 terms
The number of reflections (All/observed)	885/861	885/875
Among them: Main	91/91	
The 1st order satellites	175/171	
The 2nd order satellites	179/177	
The 3rd order satellites	172/167	
The 4th order satellites	178/172	
The 5th order satellites	90/83	
No. of refined parameters/refined atomic parameters	137/112	146/121
R and R_w (%) for Brag reflections (R_{all}/R_{obs})	1.72/1.69and 1.97/1.94	2.27/2.20 and 3.19/3.18
Among them:		
Main	1.29/1.29 and 1.66/1.66	
The 1st order satellites	2.08/2.06 and 2.11/2.09	
The 2nd order satellites	1.98/1.96 and 2.08/2.06	
The 3rd order satellites	2.31/2.22 and 1.90/1.87	
The 4th order satellites	2.12/2.06 and 1.79/1.75	
The 5th order satellites	2.40/2.27 and 2.44/2.37	
R_P and R_{wP}; R_{exp}	2.41 and 3.24; 2.99	2.62 and 3.41; 2.99
Goodness of fit (ChiQ)	1.08	1.14
Max./min. residual density (e) (Å^{-3})	0.17/−0.23	0.23/−0.27

q=0.3**a***–0.9**b***. The indexation scheme of the [001]* ED pattern is shown in Fig. 3.

3.4. Validating the model

Commensurately modulated structures can be solved either by the superspace description (basic atom positions+modulation waves) or by the traditional 3D description with an *N*-fold supercell, $N \leq n_1 \times n_2 \times n_3$, n_1, n_2 and n_3 being denominators of the rational components of the modulation vector $q = (1/n_1, 1/n_2, 1/n_3)$. Both approaches are alternative descriptions of the same structure [21]. We solved the LZNO structure from synchrotron powder diffraction data by using the superspace (3+1)D model and refined it in both the traditional 3D (supercell) and superspace (3+1)D description. The *JANA2006* program package has been used for all calculations (Table 1).

3.4.1. Refinement of commensurately modulated structure model

The fractional coordinates of the α-PbO_2 structure (S.G. *Pbcn*) were used as the initial parameters for the refinement of the average LZNO structure with all cation and anion positions assumed to be fully occupied. The atom coordinates of α-PbO_2 in the *Pbcn* space group model were transformed to a structure model with space group $P112_1/n$. As a result of this transformation lead and oxygen atoms occupy one and two 4-*fold* positions (symmetry 4*e*), respectively. The average structure is refined with a random distribution of Li^+, Zn^{2+} and Nb^{5+} cations ($\frac{1}{6}Li^+ + \frac{1}{6}Zn^{2+} + \frac{4}{6}Nb^{5+}$) in the cation positions of the α-PbO_2 structure. At an early stage of the refinement only the average substructure was refined together with the non-structural parameters, such as: unit cell parameters, zero point, and seventeenth background terms in a Legendre polynomial. The commensurately modulated structure solution has been obtained in the superspace group $P112_1/n(\alpha\beta0)00$ for the vector **q**=0.3**a***–0.9**b***, which confirms the ED data within the accuracy of the **b*** and **c*** axes directions (Fig. 3). This vector has been transformed to the equivalent **q**=0.3**a***+1.1**b*** by adding 2**b***. The transformation matrix mentioned above and t_0=0 fixed the commensurate case equivalent to the supercell lattice constants a=17.8358(9) Å, b=15.2924(7) Å, c=5.0363(3) Å, γ=96.607(5)° and space group $P2_1/b$, confirming the ED data. The crenel occupation modulation function of the *M* cation position consists of 9 atomic domains: *M*11, *M*12, *M*21, *M*22, *M*23, *M*24, Nb1, Nb2 and Zn1 (Fig. 4). The contribution of Nb and Zn atoms has been refined for each atomic domain. According to the refinement, domains Nb1, Nb2 and Zn1 are fully occupied by the corresponding atoms (Table 2). The occupation of *M*11=*M*12=0.33Zn+0.67Nb appears to be equal to 1. Since the Zn content has been completely fitted by *M*11 and *M*12, the Li atoms have been distributed among the *M*21, *M*22, *M*23 and *M*24 domains completing the Nb occupancy to 1. The composition of each atomic domain is given in Table 2. Atomic coordinates, Fourier amplitudes

Table 3
Atomic coordinates, isotropic displacements parameters and Fourier amplitudes obtained from the superspace refinement of the commensurately modulated $LiZnNb_4O_{11.5}$ structure ((3+1)D group $P112_1/n(\alpha\beta0)00$, a=4.72420(3) Å, b=5.72780(3) Å, c=5.03320(3) Å, γ=90.048(16)°, q=0.3a^*+1.1b^*).

Atom	Harmonics	x	y	z	U_{eq} (Å^2)
M[a]		−0.0005(4)	0.67803(9)	−0.2476(3)	0.00348(12)
		[−0.0054(2)]	[0.6681(9)]	[−0.247(3)]	
	s,1	−0.0024(3)	0.00387(19)	0.0056(5)	
	c,1	0.0135(3)	0.0020(2)	−0.0006(8)	
	s,2	0.0102(3)	−0.0025(3)	−0.0009(9)	
	c,2	0.0077(5)	0.0010(4)	−0.0022(12)	
	s,3	−0.0063(6)	−0.0009(5)	0.0039(7)	
	c,3	0.0090(4)	0.0039(4)	0.0036(5)	
	s,4	0.0003(4)	0.0009(4)	0.0019(10)	
	c,4	−0.0062(4)	−0.0024(4)	−0.0032(8)	
O1		0.2281(8)	0.6117(10)	0.0861(12)	0.0004(2)
		[0.166(13)]	[0.622(13)]	[0.128(14)]	
	s,1	−0.0042(12)	0.0015(10)	−0.0003(12)	
	c,1	−0.0018(14)	−0.0018(13)	−0.0025(10)	
	s,2	−0.0105(16)	−0.0036(18)	0.0017(17)	
	c,2	−0.0077(19)	0.0036(19)	0.0063(15)	
	s,3	−0.009(2)	0.0008(19)	0.0107(19)	
	c,3	−0.010(2)	0.010(2)	−0.018(2)	
	s,4	0.0016(18)	−0.002(2)	0.0026(19)	
	c,4	0.000(3)	−0.0082(18)	0.0013(12)	
O2[b]		−0.2326(9)	0.6180(12)	−0.5755(13)	0.0004
		[−0.255(13)]	[0.613(13)]	[−0.572(14)]	
	s,1	0.0056(14)	−0.0038(11)	0.0033(14)	
	c,1	−0.0114(17)	0.0041(16)	0.0033(13)	
	s,2	0.000(2)	−0.003(2)	0.0055(19)	
	c,2	0.003(2)	0.004(2)	−0.0052(17)	
	s,3	0.004(2)	0.021(2)	0.018(2)	
	c,3	0.029(2)	−0.011(2)	0.0086(19)	
	s,4	−0.015(2)	−0.0030(17)	0.0106(18)	
	c,4	0.024(3)	−0.007(2)	−0.0025(16)	

Harmonics are listed by term s for sinus, c for cosinus and order *n*.
For comparison, the corresponding values are given in the brackets after [32] for $MnTa_2O_6$ incommensurately modulated structure (the superspace group $P112_1/n(\alpha\beta0)00$ a=4.7472(2) Å, b=5.7453(3) Å, c=5.1496(3) Å, γ=90.023(9)°, **q**=−0.1038**a***+0.691**b***).

[a] *M* refers cation position described by Crenel occupation modulation (see Table 2 and Fig. 4).

[b] Occupancy 0.918 is modulated with Fourier amplitudes s,1=0.033(9), c,1=0.011(8), s,2=0.006(9) and c,2=0.082(12) (see Fig. 5).

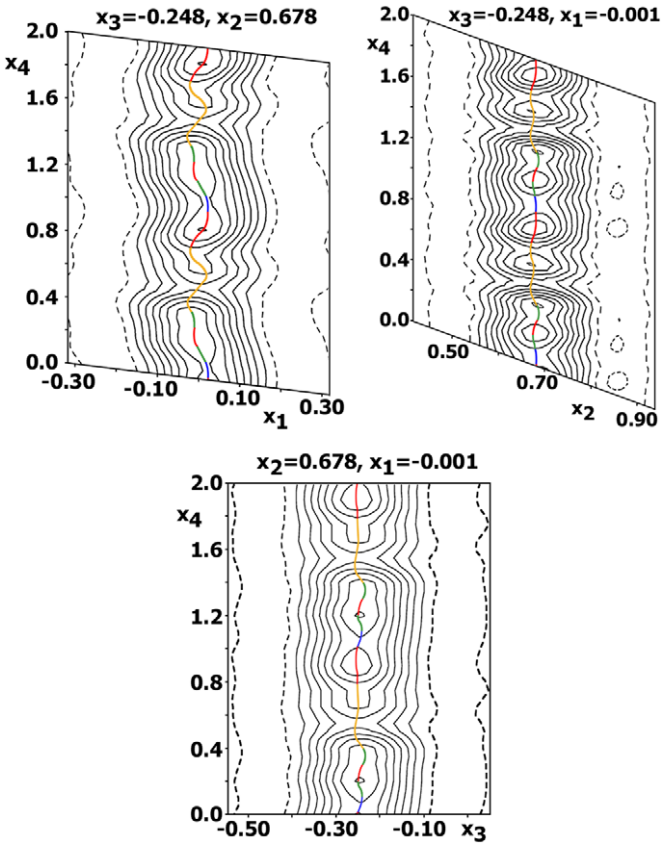

Fig. 5. (Colour online). Positional modulations of Li, Zn, and Nb in $LiZnNb_4O_{11.5}$ as a function of the internal x_4 axis in the Fourier syntheses of electron density calculated in the vicinity of the cation position. The step between lines is 10 e/cm^3. The central coloured lines correspond to the calculated atomic positions (yellow—Li/Nb positions *M*21–*M*24; blue—Zn positions; red—Nb positions, green—Zn/Nb positions *M*11–*M*12).

of the displacive modulations and isotropic displacement parameters (Table 3) have been constrained as identical for all cationic domains. The obtained cation distribution is in good agreement with the electron density calculated around the cation position (Fig. 5). Refinement of the occupancy of the O atoms reveals a deficiency (1–0.918) and a modulation for O2 (Fig. 6 and Table 3), while the occupancy of O1 exhibits no essential deviation from 1. Only 4 among the 10 O2 positions are characterized by an occupancy less than 1 within 3 standard deviations (Fig. 6). The main characteristics of the structure refinement are listed in Table 1. The calculated and residual XRD patterns are shown in Fig. 7. The *ab* projection of the structure obtained with the superspace model is shown in Fig. 8. The cation–oxygen distances are plotted as function of *t* in Fig. 9 and listed in Table 5.

3.4.2. *Refinement of the supercell model*

The supercell model with space group $P2_1/b$ and unit cell parameters $a=17.8358(9)$ Å, $b=15.2924(7)$ Å, $c=5.0363(3)$ Å, $\gamma=96.607(5)^\circ$ has been derived from the superspace model using the matrix mentioned above. Nine cation domains have been transformed into 10 independent atomic positions keeping the corresponding occupancies, which have been further refined along with positional and individual isotropic displacement parameters. Two independent O-positions of the superspace model have been transformed into 20 independent positions in the supercell model. Occupancies obtained from the superspace model were kept, while the positional parameters were refined

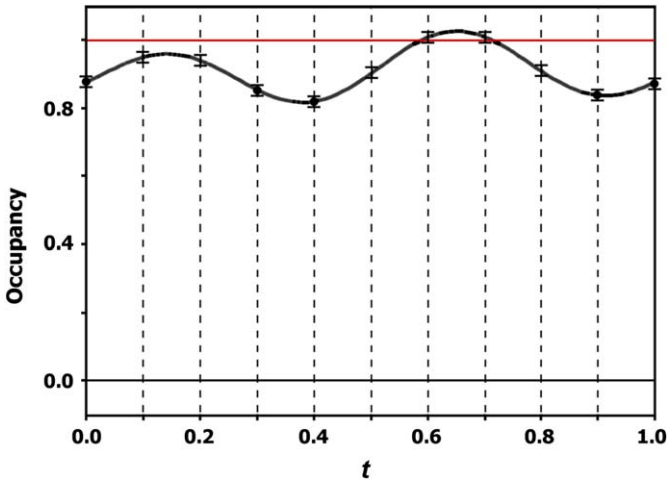

Fig. 6. O_2 occupancy modulation as a function of *t*. Only 10 points corresponding to intersections of the function with dashed lines refer to the commensurately modulated structure of $LiZnNb_4O_{11.5}$. The standard deviations (sd) are indicated. Occupation of four positions of O_2 (marked with black points) deviate from 1 within 3 sd.

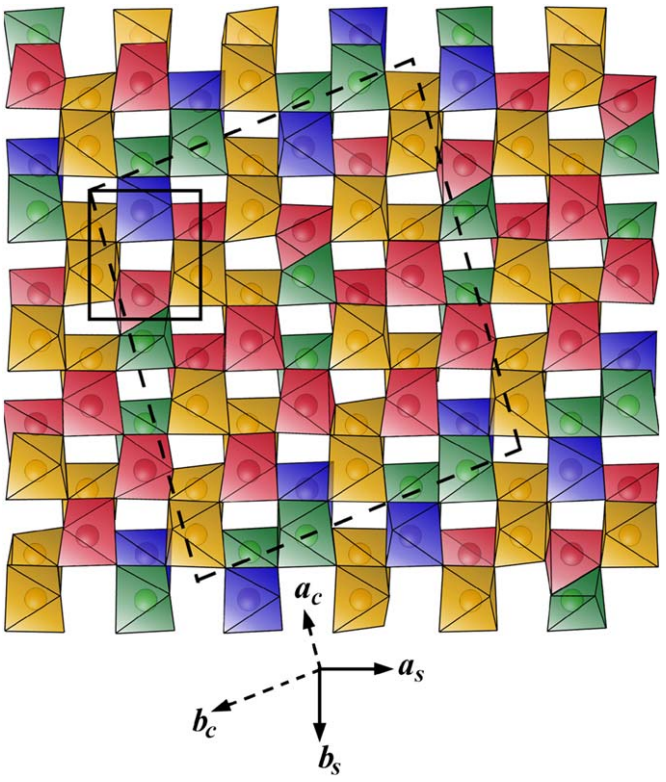

Fig. 8. (Colour online). Polyhedral view of the of $LiZnNb_4O_{11.5}$ crystal structure along the *c* axis (yellow—polyhedra of *M*21–*M*24 positions occupied by Li^+ and Nb^{5+} cations; blue—ZnO_6 polyhedra; red—NbO_6 polyhedra, green—polyhedra of *M*11–*M*12 positions occupied by Zn^{2+} and Nb^{5+} cations). The subcell (marked as s) and supercell (marked as c) are indicated by solid and dashed lines, respectively.

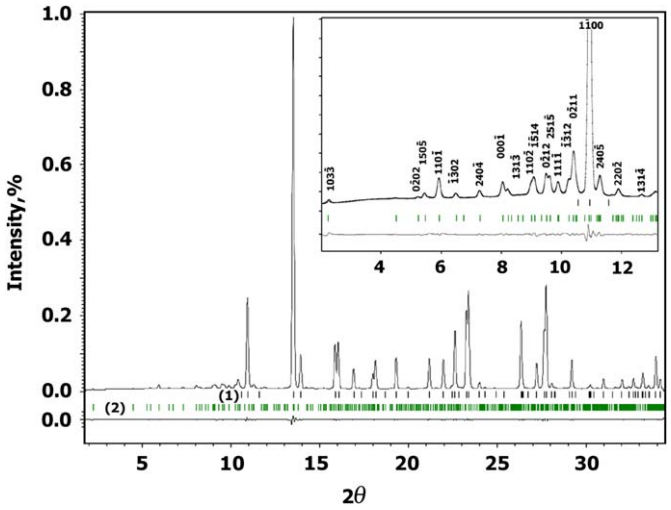

Fig. 7. (Colour online). Calculated and residual X-ray diffraction patterns $LiZnNb_4O_{11.5}$, obtained from superspace model. Main and satellites reflections are identified as (1) (black lines) and (2) (green lines), respectively.

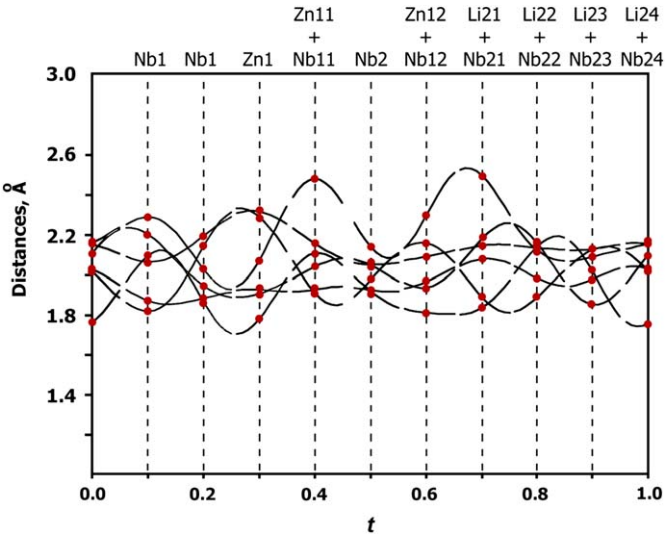

Fig. 9. *t* dependence of the Li–O, Zn–O and Nb–O distances in $LiZnNb_4O_{11.5}$.

Table 4
Occupation factors (*occ.*), atomic coordinates and isotropic atomic displacements parameters obtained from the refinement of $LiZnNb_4O_{11.5}$ structure in supercell (space group $P2_1/b$, a=17.8358(9) Å, b=15.2924(7) Å, c=5.0363(3) Å and γ=96.607(5)°).

Atom	*occ.*	*x*	*y*	*z*	U_{eq} (Å^2)
*M*11	0.333 Zn+0.667(3) Nb	0.59738(19)	0.4718(3)	0.7493(15)	0.0144(10)
*M*12	0.3333 Zn+0.667(3) Nb	0.9936(2)	0.6652(2)	0.7654(15)	0.0136(11)
*M*21	0.1897Li+0.810(3)Nb	0.69454(18)	0.7595(2)	0.7589(15)	0.002(1)
*M*22	0.6516Li +0.348(4)Nb	0.3966(5)	0.8698(6)	0.748(4)	0.0016(12)
*M*23	0.315Li+0.685(4)Nb	0.0999(2)	0.9716(3)	0.7524(19)	0.002(1)
*M*24	0.5Li +0.50(1)Nb	0.7976(3)	0.0630(4)	0.752(3)	0.002(2)
Nb1	1	0.19717(16)	0.2750(2)	0.7458(14)	0.0016(10)
Nb2	1	0.49548(18)	0.1675(2)	0.7472(16)	0.0047(9)
Nb3	1	0.29524(16)	0.5659(2)	0.7516(14)	0.0032(8)
Zn1	1	0.8988(3)	0.3737(3)	0.7537(16)	0.0012
O1–1	1	0.8389(12)	0.1203(11)	0.092(3)	0.0007(4)
O1–2	1	0.9367(12)	0.4225(13)	0.080(4)	0.0007
O1–3	1	0.0444(12)	0.7312(13)	0.091(3)	0.0007
O1–4	1	0.1438(11)	0.0322(13)	0.067(4)	0.0007
O1–5	1	0.2451(11)	0.3351(13)	0.079(4)	0.0007
O1–6	1	0.3424(11)	0.6302(12)	0.068(4)	0.0007
O1–7	1	0.4417(14)	0.9332(13)	0.094(3)	0.0007
O1–8	1	0.5423(12)	0.2363(13)	0.079(4)	0.0007
O1–9	1	0.6358(11)	0.5280(12)	0.093(4)	0.0007
O1–10	1	0.7320(11)	0.8296(11)	0.093(4)	0.0007
O2–1	0.8842	0.7871(12)	0.9809(14)	0.425(4)	0.0007
O2–2	0.8617	0.8888(12)	0.2857(15)	0.379(4)	0.0007
O2–3	1	0.9961(12)	0.5869(11)	0.400(4)	0.0007
O2–4	0.861	0.0935(15)	0.8964(15)	0.406(4)	0.0007
O2–5	0.9471	0.1928(13)	0.1941(13)	0.421(4)	0.0007
O2–6	0.909	0.2775(11)	0.4828(12)	0.454(4)	0.0007
O2–7	0.9158	0.3940(15)	0.7918(15)	0.417(3)	0.0007
O2–8	0.9575	0.4896(13)	0.1003(14)	0.449(4)	0.0007
O2–9	0.8436	0.5947(14)	0.4056(15)	0.432(3)	0.0007
O2–10	1	0.6931(11)	0.7010(13)	0.445(3)	0.0007

for all 20 O-positions; isotropic displacement parameters have been constrained as equivalent for all O atoms. The resulting characteristics of all atomic positions are listed in Table 4. The characteristics of the structure refinement are shown in Table 1. The cation–oxygen distances are listed in Table 5.

Supplementary material has been sent to the Fachinformationzentrum Karlsruhe, Abt. PROKA, 76344, Eggenstein-Leopoldshaften, Germany, as supplementary materials CSD numbers 420842 (superspace) and 420832 (supercell) and can be obtained by contacting the FIZ (quoting the article details and the corresponding SUP number).

3.5. High resolution transmission electron microscopy

A HRTEM study has been performed along the $[001]_s$ and $[310]_s$ direction (Fig. 10a and b, respectively), of the commensurate modulated LZNO where the structure can be interpreted in terms of cation and oxygen columns (Fig. 10). As confirmed by the image simulation, dark dots in the $[001]_s$ image correspond to the projection of cation columns while the brighter dots represent channels in the structure (Fig. 10a). The positional parameters of the supercell model obtained from the refinement of the X-ray synchrotron powder data were taken as an input to simulate the HREM images. The calculated images for a defocus value $\Delta f = -40$ nm and t=7 nm (*a*), Δf=10 nm and a thickness t=10 nm (*b*) are shown as an inset and show a good agreement between the experimental and calculated image. The brightest dots rows are separated by 17 Å which corresponds to $a^*\cos(\gamma - 90)$ of the $LiZnNb_4O_{11.5}$ basic structure. However, two interlayer spacings, different from the basic structure, have been found suggesting the presence of planar defects or other related structures.

A HRTEM image of such a defect (termed anion-deficient (AD)) having a larger layer separation (around 20 Å, marked by a white arrow) is shown in Fig. 10 viewed along two different zone axes. Obviously, apart from a different spacing, the contrast is similar to the basic structure image, suggesting a structural model as presented in Fig. 12a. Missing a block in the stacking consisting of three layers (Nb2, Nb3, *M*22 (0.3333Zn+0.667Nb) and *M*22 (0.6516Li +0.348Nb)) will lead to the merging of two neighbouring unit cells and the occurrence a larger unit cell with approximate composition $Li_{0.67}Zn_{0.75}Nb_{2.58}O_{7.5}$ and unit cell parameters: $a_{AD}\sim 20$ Å, $b_{AD}\sim 15.3$ Å, $c_{AD}\sim 5.0$ Å and $\gamma\sim 93°$.

Another type of defect (termed cation-deficient (CD)) with a smaller *c*-parameter ($\sim$12.8 Å) is also observed and is caused by a different structural block stacking. The missing block in this case consists of other three layers: Zn, *M*12 (0.3333Zn+0.667Nb) and *M*21 (0.1897Li+0.810Nb) (Fig. 12b) and the approximate composition is $Li_{0.84}Zn_{0.19}Nb_{2.96}O_8$. It should be noticed that this type of the defect tends to appear in blocks (2 or 3 units of 12.8 Å) (Fig. 11a) which allow us to consider this structure as a new phase in the Li_2O–ZnO–Nb_2O_5 system with a nominal composition of $Li_{0.84}Zn_{0.19}Nb_{2.96}O_8$ and unit cell parameters: $a_{CD}\sim 12.8$ Å, $b_{CD}=b_{AD}\sim 15.3$ Å, $c_{CD}\sim 5.0$ Å and $\gamma\sim 90°$.

Such local structural and chemical inhomogeneities, will introduce anti-phase boundaries (APBs) that will compensate for the mismatch between different stacking fault structures. Fig. 11b shows a $[001]_s$ HRTEM image of such APB. The APB exhibits a good coherence across the boundary and can be described as a shift of the cation layers with respect to each other with displacement vector $\boldsymbol{R}=(110)_s$. The mismatch along the boundary implies the presence of a locally distorted structure with a somewhat different atomic bonding or cation rearrangement. A structural model of such APB is shown in Fig. 12c. The

Table 5
Cation–oxygen distances (Å) obtained from structure refinement using both superspace and supercell models.

Superspace		Supercell	
Distance	d (Å)	Distance	d (Å)
*M*11–O1	2.04(4)	*M*11–O1–9	2.015(19)
–O1(i)	1.92(4)	–O1–7	1.85(2)
–O1(ii)	2.15(4)	–O1–6	2.19(2)
–O2	1.91(4)	–O2–9	1.89(2)
–O2(iii)	2.10(4)	–O2–8	2.06(2)
–O2(iv)	**2.47(4)**	–O2–9	**2.479(19)**
⟨*M*11–O⟩	2.10	⟨*M*11–O⟩	**2.08**
*M*12–O1	1.93(4)	*M*12–O1–3	2.00(2)
–O1(i)	1.96(4)	–O1–3	2.077(19)
–O1(ii)	2.08(4)	–O1–2	2.08(2)
–O2	2.15(4)	–O2–3	2.189(19)
–O2(iii)	1.80(4)	–O2–4	1.86(2)
–O2(iv)	2.29(4)	–O2–2	2.26(12)
⟨*M*12–O⟩	2.04	⟨*M*12–O⟩	2.08
*M*21–O1	2.18(4)	*M*21–O1–6	2.11(2)
–O1(i)	2.07(4)	–O1–10	2.065(19)
–O1(ii)	2.14(4)	–O1–5	2.07(2)
–O2	1.89(4)	–O2–7	1.86(2)
–O2(iii)	1.83(4)	–O2–10	1.814(19)
–O2(iv)	**2.49(4)**	–O2–5	2.24(2)
⟨*M*21–O⟩	2.10	⟨*M*21–O⟩	2.03
*M*22–O1	2.16(4)	*M*22–O1–8	2.23(2)
–O1(i)	1.98(4)	–O1–9	1.90(2)
–O1(ii)	2.13(4)	–O1–7	2.11(2)
–O2	1.88(4)	–O2–7	2.05(3)
–O2(iii)	2.14(4)	–O2–8	2.26(2)
–O2(iv)	2.12(4)	–O2–10	2.08(2)
⟨*M*22–O⟩	2.07	⟨*M*22–O⟩	2.11
*M*23–O1	1.85(4)	*M*23–O1–4	1.95(2)
–O1(i)	1.98(4)	–O1–2	2.01(2)
–O1(ii)	2.13(4)	–O1–1	2.03(2)
–O2	2.12(4)	–O2–1	2.25(2)
–O2(iii)	2.02(4)	–O2–3	1.98(2)
–O2(iv)	2.09(4)	–O2–4	2.09(2)
⟨*M*23–O⟩	2.03	⟨*M*23–O⟩	2.05
*M*24–O1	2.10(4)	*M*24–O1–1	2.02(2)
–O1(i)	2.03(4)	–O1–5	2.01(2)
–O1(ii)	2.15(4)	–O1–4	2.09(2)
–O2	2.02(4)	–O2–1	2.06(2)
–O2(iii)	1.76(4)	–O2–6	1.76(2)
–O2(iv)	2.16(4)	–O2–	2.12(3)
⟨*M*24–O⟩	2.04	⟨*M*24–O⟩	2.01
Nb3–O1	2.05(4)	Nb3–O1–6	2.005(19)
–O1(i)	1.93(4)	–O1–10	1.898(19)
–O1(ii)	2.05(4)	–O1–9	2.14(2)
–O2	1.98(4)	–O2–6	1.968(19)
–O2(iii)	1.92(4)	–O2–1	1.79(2)
–O2(iv)	2.14(4)	–O2–9	2.17(2)
⟨Nb3–O⟩	2.01	⟨Nb3–O⟩	2.00
Zn1–O1	1.90(4)	Zn1–O1–2	1.89(2)
–O1(i)	1.92(4)	–O1–4	1.95(2)
–O1(ii)	2.31(4)	–O1–3	2.14(2)
–O2	2.28(4)	–O2–2	2.31(2)
–O2(iii)	1.77(4)	–O2–5	2.02(2)
–O2(iv)	2.06(4)	–O2–3	2.05(2)
⟨Zn1–O⟩	2.04	⟨Zn1–O⟩	2.06
Nb1a–O1	2.20(4)	Nb1–O1–5	2.05(2)
–O1(i)	1.88(4)	–O1–1	1.952(19)
–O1(ii)	2.20(4)	–O1–10	2.296(19)
–O2	2.14(4)	–O2–10	2.17(2)
–O2(iii)	1.86(4)	–O2–2	1.82(2)
–O2(iv)	2.03(4)	–O2–5	2.05(2)
⟨Nb1a–O⟩	2.05	⟨Nb1–O⟩	2.06
Nb1b–O1	1.95(4)	Nb2–O1–8	2.09(2)
–O1(i)	1.87(4)	–O1–8	1.89(2)
–O1(ii)	2.07(4)	–O1–7	2.16(2)
–O2	1.82(4)	–O2–8	1.81(2)
–O2(iii)	2.10(4)	–O2–9	2.07(2)
–O2(iv)	2.29(4)	–O2–7	2.16(3)
⟨Nb1b–O⟩	2.02	⟨Nb2–O⟩	2.03

Symmetry codes: (i) $x+1/2,-y+3/2,z-1/2$; (ii) $-x,-y+1,-z$; (iii) $-x-1/2,-y+3/2,z+1/2$; (iv) $-x,-y+1,-z-1$

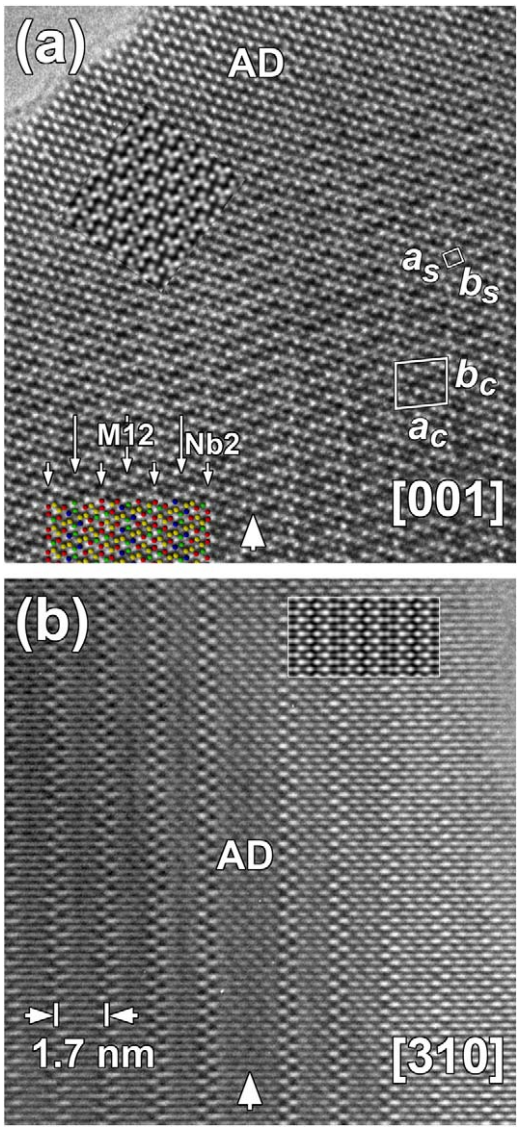

Fig. 10. (Colour online). HRTEM images of the commensurate modulated $LiZnNb_4O_{11.5}$ structure along $[001]_s$—(a) and $[310]_s$—(b) zones. The calculated images for a defocus value $\Delta f = -40$ nm and $t = 7$ nm (*a*), $\Delta f = 10$ nm and a thickness $t = 10$ nm (*b*) are shown as an inset. The subcell (denoted as "s") and supercell (denoted as "c") are shown. The structural model (only cations are presence for simplicity) overlay on experimental HRTEM image where colour circles correspond to the following cations: yellow—Li/Nb positions *M*21–*M*24; blue—Zn positions; red—Nb positions, green—Zn/Nb positions *M*11–*M*12.

boundary is formed by blocks of two chains which build up vertex-sharing four NbO_6 octahedra and four $(Li/Nb)O_6$ octahedra, respectively. The $\{NbO_6\}_4$ and $\{(Li/Nb)O_6\}_4$ chains connect via common edges.

4. Discussion

4.1. Comparing the superspace and supercell structure refinement

As it can be deduced from Table 1, the superspace model is characterized by essentially lower values of structural *R*-factors along with lower numbers of refined parameters. The refined compositions of the cation positions are qualitatively identical and quantitatively differ within 3–4 standard deviations for only *M*21, *M*22 and *M*23 containing Li atoms (compare Table 2 and 4). Comparison of the O atomic positions can be estimated using the

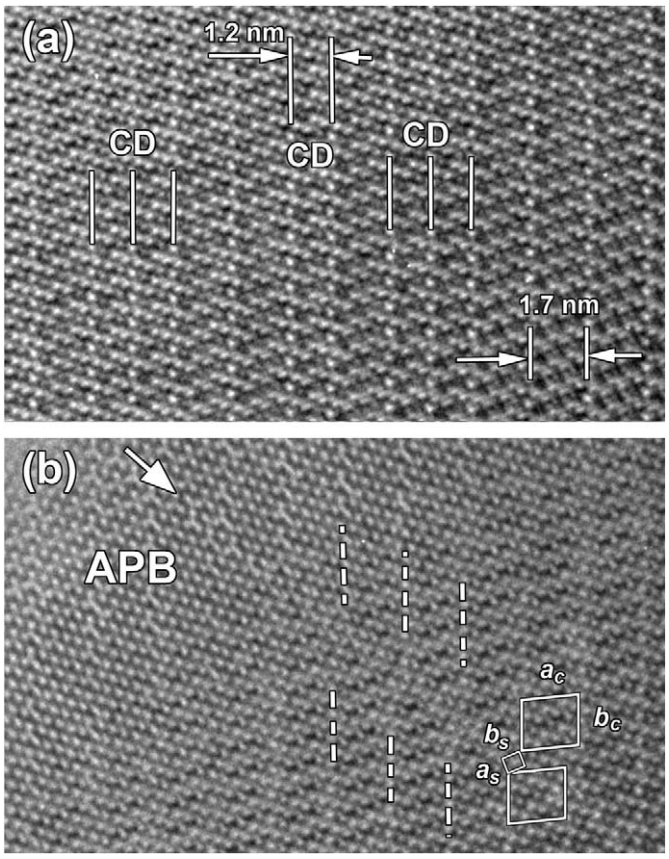

Fig. 11. (a) $(001)_s$ HRTEM images of the cation-deficiency type defect and (b)—the anti-phase boundary (APB) (marked by white arrow).

cation–oxygen distances listed in Table 5 for both models. As can be seen, the distances are identical within 0–3 standard deviations. Therefore, one can conclude that the crystal structure of LZNO could be refined with identical results using both superspace and supercell approach. The lower number of refined parameters characteristic of the superspace model leads to higher values of standard deviations in comparison to the supercell model. However, this does not mean that the parameters of the supercell model are more accurate; actually the superspace model gives a more realistic estimation of these parameters. Taken into account also the lower values of all *R*-factors, the superspace refinement is more efficient.

4.2. The α-PbO_2-*Z* (3+1)-dimensional structure type

The LNZO structure is the second one, which has been solved and refined in the superspace group $P112_1/n(\alpha\beta0)00$ with α-PbO_2-like subcell constants. First was the high-temperature and high-pressure (HT-HP) modification of $MnTa_2O_6$, which has been reported [22] as an incommensurately modulated structure with similar atomic coordinates (Table 3). The LNZO and HT-HP-$MnTa_2O_6$ structures differ by the modulation vector **q**, which is equal to $-0.1038\mathbf{a}^*+0.691\mathbf{b}^*$ for the incommensurately modulated $MnTa_2O_6$ and $0.3\mathbf{a}^*+1.1\mathbf{b}^*$ for the commensurately modulated LZNO. The occupation modulation function of the *M* position is also different (Table 2 and 6). Three other groups of known α-PbO_2 related structures can be also described with the superspace group $P112_1/n(\alpha\beta0)00$, similar subcell and atomic sites, but with different **q** vectors and occupation modulation

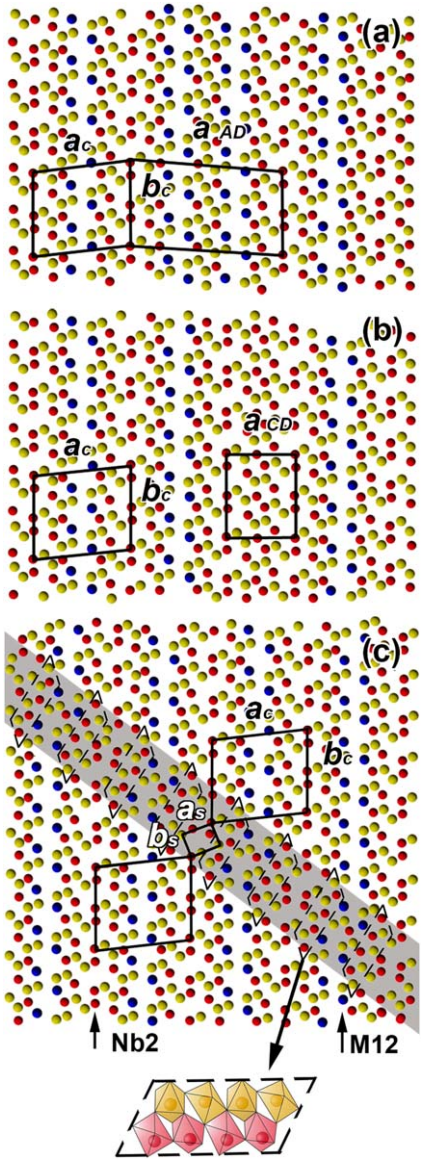

Fig. 12. (Colour online). Structural models of defects formations in $LiZnNb_4O_{11.5}$ structure: (a) oxygen-deficiency (b) cation-deficiency; (c) anti-phase boundary. The a_{AD} and a_{CD} correspond to the unit cell parameters anion-deficient and cation-deficient phases, respectively. The colour circles correspond to: yellow—Li/Nb; blue—Zn positions; red—Nb atoms. Note the building blocks marked by dash line frame repeated along APB.

function of the *M* site (Table 6). The corresponding structures with indication of their supercell and subcell are shown in Fig. 13.

Two analogous structural families have already been described as the scheelite (3+1)D structure type [23] and the calaverite (3+1)D structure type [24]. By analogy, the α-PbO_2 related compounds described with the $P112_1/n(\alpha\beta0)00$ superspace group can be referred to the α-PbO_2-*Z* (3+1)D structure type, where *Z* specifies the *c* monoclinic axis inherited from the *Pbcn* space group characteristic of α-PbO_2. In contrast to that, there is a group of α-PbO_2 related compounds, such as wolframites, AWO_4 (*A*=Mn, Fe, Cu, Zn), Wodginites, $MnA(Nb,Ta)_2O_8$ (*A*=Sn, Ta, Ti, Fe, Li, Zr) [22], with the *b* monoclinic axis inherited from the α-PbO_2 space group. This group could be described in the α-PbO_2-*Y* (3+1)D structure type, probably with $P12/c1(\alpha0\gamma)00$ superspace group. As it can be deduced from Table 6, the α-PbO_2-*Z* (3+1)D structure type joins 4 different 3D structure types and one incommensurately modulated structure, which can be referred only to a higher

Table 6
Some α-PbO_2 related compounds describing in α-PbO_2-*Z* (3+1)D structure type.

Compound [Ref.]	Supercell model Space group; supercell constants *a*, *b*, *c* (Å), γ (°); number *N* of independent atomic sites	Superspace model $P112_1/n(\alpha\beta0)00$ superspace group; subcell constants $a \approx 4.7$ Å, $b \approx 5.7$ Å, $c \approx 5.03$ Å, $\gamma \cong 90^\circ$; $N=3$ independent atomic sites: *M* (4e: ≈0, 0.68, 0.75); O1 (4e: ≈0.2, 0.6, 0.1); O2 (4e: ≈0.75, 0.62, 0.43)
	Modulation vector $\mathbf{q}=\alpha\mathbf{a}^*+\beta\mathbf{b}^*$	The lengths, Δ, of the atomic domains in the crenel occupation function of the *M* site; *O*1=0 and *O*2=0.5 are the centres of domains in the *t* translation
Incommensurate member		
HT-HP-$MnTa_2O_6$ [22]	none	$-0.1038\mathbf{a}^*+0.691\mathbf{b}^*$ $\Delta_{M1}=0.293$; $\Delta_{M2}=0.707$; *M*1=0.78Mn+0.22Ta; *M*2=0.148Mn+0.852Ta
Commensurate members		
$LiZnNb_4O_{11.5}$ [present work]	$P2_1/b$; 17.84, 15.29, 5.04, 96.61; $N=30$	$\mathbf{q}=0.3\mathbf{a}^*+1.1\mathbf{b}^*$ (see Table 2)
$LiNb_3O_8$[a] [15] (and R_3ReO_8, *R*=Pr [25], Y [26], Sm [27]; $CuNb_3O_8$ [28])	$P2_1/b$; 7.46, 15.26, 5.03, 107.34; $N=12$	$\mathbf{q}=0.25\mathbf{a}^*+1.25\mathbf{b}^*$ $\Delta_{Li(Re,Cu)}=1/4$, $\Delta_{Nb(R}=3/4$
$ZnNb_2O_6$[a] [10] ($MgNb_2O_6$ structure type)	*Pbcn*[b]; 14.2, 5.7, 5.04, 90; $N=5$	$\mathbf{q}=2/3\mathbf{a}^*+0\mathbf{b}^*$ $\Delta_{Zn}=1/3$, $\Delta_{Nb}=2/3$
$ZnTa_2O_6$[a] [10] (Fe_2WO_6 structure type)	*Pbcn*[b]; 4.7, 17.1, 5.07, 90; $N=6$	$\mathbf{q}=0\mathbf{a}^*+4/3\mathbf{b}^*$; $t_0=0$ $\Delta_{Zn}=2/3$, $\Delta_{Ta}=1/3$

[a] $T=(-1\ 1\ 0/3\ 1\ 0/0\ 0\ -1/)$ for $LiNb_3O_8$, $(3\ 0\ 0/0\ -1\ 0/0\ 0\ -1)$ for $ZnNb_2O_6$ and $(1\ 0\ 0/0\ -3\ 0/0\ 0\ -1)$ for $ZnTa_2O_6$ in the matrix equation $A_{supersell}=A_{subcell}T$.
[b] Space group $P112_1/n$ with monoclinic angle $\gamma=90^\circ$ corresponds to topologically identical structures derived from the superspace model.

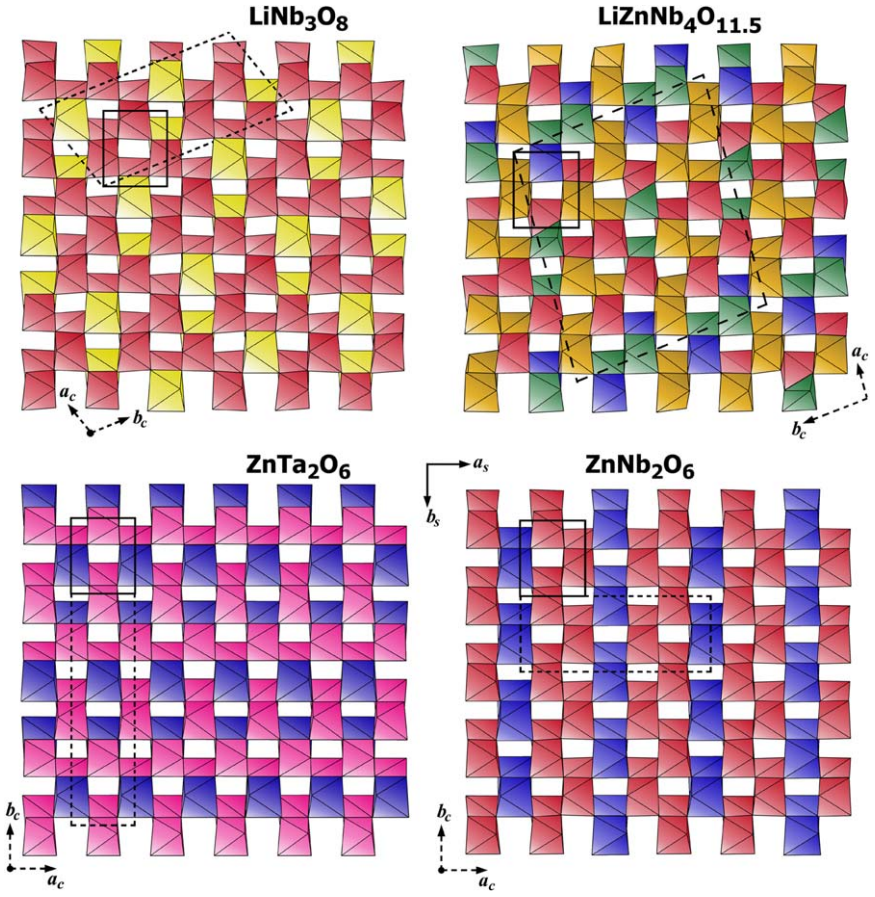

Fig. 13. (Colour online). The *ab* projection of some commensurately modulated structures of the α-PbO_2-*Z* (3+1)D structure type (yellow—LiO_6 polyhedra; dark yellow—(Li,Nb) polyhedra; blue—ZnO_6 polyhedra; red—NbO_6 polyhedra, green—(Zn,Nb) polyhedra, purple—TaO_6 polyhedra). The common subcell (basic cell) and supercells are indicated by dashed and solid lines, respectively.

dimension type because of the absence its 3D symmetry. Taken into account the supercell parameters and space group (Table 1), LZNO has a new 3D structure type. $LiNb_3O_8$ [15] is isotypic with R_3ReO_8, where *R*=Pr [25], Y [26], Sm [27], and $CuNb_3O_8$ [28]. $ZnNb_2O_6$ [8] belongs to the $MgNb_2O_6$ [29] structure type fitting more than 60 $A(Nb,Ta)O_6$ compositions (*A*=Mg, Fe, Mn, Sn, Ca, Ti, Y, Cu, Ce, Zn, U, Ni, Co), including natural columbites/tantalites. $ZnTa_2O_6$ [10] has the Fe_2WO_6 [30] structure type matching seven

compounds in the ICSD database. Therefore, the α-PbO_2-*Z* (3+1)D structure type allows a unified representation of more than 70 compounds. It should be mentioned that within this (3+1)D structure type the $MgNb_2O_6$ and FeW_2O_6 groups can both be characterized by only a monoclinic symmetry, which is however a subgroup of their orthorhombic space group (Table 6). On the one hand, this limits the symmetrical capacity of the superspace model; on the other hand, the lower symmetry derived from the superspace group points to the probability of lower symmetry under some specific conditions. Indeed, the HT-HP-modification of $MnTa_2O_6$ exhibits a monoclinic symmetry [22], while the room temperature modification [31] is isotypic with the orthorhombic α-PbO_2.

5. Conclusions

A novel lithium zinc niobium oxide $LiZnNb_4O_{11.5}$ has been found in the Nb-rich part of the Li_2O–ZnO–Nb_2O_5 system; it has a novel α-PbO_2 related structure. The compound has been synthesized by the routine ceramic technique and characterized by X-ray diffraction and transmission electron microscopy. All reflections in XRD and ED patterns for LZNO can be indexed in the monoclinic space group $P2_1/b$ with supercell parameters a=17.8358(9) Å, b=15.2924(7) Å, c=5.0363(3) Å, γ=96.607(5)° or in the superspace group $P112_1/n(\alpha\beta0)00$ with subcell parameters a=4.72420(3) Å, b=5.72780(3) Å, c=5.03320(3) Å and γ=90.048(16)° and a rational value of the modulation vector $\mathbf{q}=0.3\boldsymbol{a}^*+1.1\boldsymbol{b}^*$. The structure has been solved and refined by the Rietveld method from synchrotron powder diffraction data using both superspace and traditional supercell models. The superspace description allows to consider the LZNO structure as a member of the α-PbO_2-*Z* (3+1)D structure type family uniting one incommensurately modulated and 4 groups of commensurately modulated α-PbO_2 related structures, which differ by the coefficients α and β in $\mathbf{q}=\alpha\boldsymbol{a}^*+\beta\boldsymbol{b}^*$ and in the occupation modulation function of the cation position *M*. The subcell constants ($a\approx4.7$ Å, $b\approx5.7$ Å, $c\approx5.03$ Å, $\gamma\cong90°$) and 3 atomic sites (*M*: 4e (≈0, 0.68, 0.75); O1: 4e (≈0.2, 0.6, 0.1); O2: 4e (≈0.75, 0.62, 0.43)) are similar in the unique $P112_1/n(\alpha\beta0)00$ superspace group for all (about 70) structures of the α-PbO_2-*Z* (3+1)D structure type.

HRTEM revealed several types of defects in LZNO (anion- and cation-deficient defects as well as anti-phase boundaries); structural models for the formation these defects are proposed. The presence of these defects allows us to predict the formation of two new phases in the Li_2O–ZnO–Nb_2O_5 system.

Acknowledgments

The authors are grateful to the Russian Foundation for Basic Research (Grant 07-03-01054) for financial support. This work has been performed within the framework of IAP-VI of the Belgian government. A. Arakcheeva and G. Chapuis are grateful to the support of the Swiss National Science foundation, (Grants no. 20-105325/1 and 200021-109470/1).

References

[1] [a] A. Rauber, in: E. Kaldis (Ed.), Current Topics in Material Science, vol. 1, North-Holland, Amsterdam, 1978, pp. 481–601;
[b] L. Wooten, K.M. Kissa, A. Yi-Yan, E.J. Murphy, D.A. Lafaw, P.F. Hallemeier, D. Maack, D.V. Attanasio, D.J. Fritz, G.J. McBrien, D.E. Bossi, IEEE J. Sel. Top. Quant. Electron. 6 (2000) 69;
[c] Y. Zhu, J. Zhang, T. Yi, Q. Gong, Opt. Commun. 281 (2008) 1450;
[d] J.M. Cabrera, J. Olivares, M. Carrascosa, J. Rams, R. Muller, E. Dieguez, Adv. Phys. 45 (1996) 349;
[e] M. Pierrou, F. Laurell, H. Karlsson, T. Kellner, C. Czeranowsky, G. Huber, Opt. Lett. 24 (1999) 205;
[f] R.S. Weis, T.K. Gaylord, Appl. Phys. A 37 (1985) 191.
[2] P.F. Bordui, R.G. Norwood, C.D. Bird, G.D. Calvert, J. Cryst. Growth 113 (1991) 61.
[3] U. Schlarb, M. Wohlecke, B. Gather, A. Reichert, K. Betzler, T. Volk, N. Rubinina, Opt. Mater. 4 (1995) 791.
[4] D.A. Bryan, R. Gerson, H.E. Tomaschke, Appl. Phys. Lett. 44 (1984) 847.
[5] T.R. Volk, V.I. Pryalkin, N.M. Rubinina, Opt. Lett. 15 (1990) 996.
[6] [a] C. Gonzalez, M.L. Lopez, M. Gaitan, M.L. Veiga, C. Pico, Mater. Res. Bull. 29 (1994) 903;
[b] S.J. Marin, M. O'Keeffe, D.E. Partin, J. Solid State Chem. 113 (1994) 413;
[c] M. Ferriol, S. Lecocq, Eur. J. Solid State Inorg. Chem. 35 (1998) 707.
[7] Powder Diffraction File, Card 53-0343, JCPDS; International Center for Diffraction Data, 1601 Park Ln., Swartmore, PA 19081.
[8] A.J. Pollard, J. Am. Ceram. Soc. 44 (1961) 630.
[9] A.A. Ballman, H. Brown, J. Cryst. Growth 41 (1977) 36.
[10] M. Waburg, Hk. Mueller-Buschbaum, Z. Anorg. Allg. Chem. 508 (1984) 55.
[11] H.J. Goldschmidt, Metallurgia 62 (1960) 211.
[12] R.W. Harrison, E.J. Delgrosso, J. Electrochem. Soc. 110 (1963) 205.
[13] N.V. Tarakina, A.P. Tyutyunnik, V.G. Zubkov, T.V. D'yachkova, Y.G. Zainulin, H. Hannerz, G. Svensson, Solid State Sci. 5 (2003) 459.
[14] R. Norin, B. Dahlen, Acta Chem. Scand. 23 (1969) 1826.
[15] M. Lundberg, Acta Chem. Scand. 25 (1971) 3337.
[16] B.M. Gatehouse, P. Leverett, Cryst. Struct. Commun. 1 (1972) 83.
[17] A.T. Zaslavskii, S.S. Tolkachev, Zhur. Fiz. Khim. 26 (1952) 743 (in Russian).
[18] A.P. Hammersley, S.O. Svensson, M. Hanfland, A.N. Fitch, D. Hausermann, High Pressure Res. 14 (1996) 235.
[19] H.M. Rietveld, J. Appl. Crystallogr. 22 (1969) 65.
[20] [a] V. Petrícek, M. Dusek, L. Palatinus, JANA2000: the crystallographic computing system, Institute of Physics, Praha, Czech Republic, 2000;
[b] M. Dusek, V. Petrícek, M. Wunschel, R.E. Dinnebier, S. van Smaalen, J. Appl. Cryst. 34 (2001) 398;
[c] K. Brandenburg, DIAMOND, Version. 2.1c. Crystal Impact GbR, Bonn, Germany, 1999.
[21] [a] M. Dušek, G. Chapuis, M. Meyer, V. Petrichek, Acta Cryst. B 59 (2003) 337;
[b] L. Palatinus, M. Dušek, R. Glaum, B. El Bali, Acta Cryst. B 62 (2006) 556.
[22] N.V. Tarakina, A.P. Tyutyunnik, V.G. Zubkov, T.V. D'Yachkova, Y.G. Zainulina, H. Hannerz, G. Svensson, Solid State Sci. 5 (2003) 983.
[23] A. Arakcheeva, G. Chapuis, Acta Cryst. B 64 (2008) 12.
[24] L. Bindy, A. Arakcheeva, G. Chapuis, Am. Mineralogist 94 (2009) 728.
[25] W. Jeitschko, D.H. Heumannskaemper, U.C. Rodewald, M.S. Schriewer-Poettgen, Z. Anorg. Allg. Chem. 626 (2000) 80.
[26] G. Baud, J.P. Besse, R. Chevalier, M.J. Gasperin, Solid State Chem. 38 (1981) 186.
[27] J.P. Besse, M. Bolte, G. Baud, R. Chevalier, Acta Cryst. B 32 (1976) 3045.
[28] B.O. Marinder, P.E. Werner, E. Wahlstrom, G. Malmros, Acta Chem. Scand. A 34 (1980) 51.
[29] S. Pagola, R.E. Carbonio, J.A. Alonso, M.T. Fernandez-Diaz, J. Solid State Chem. 134 (1997) 76.
[30] J. Senegas, J. Galy, J. Solid State Chem. 10 (1974) 5.
[31] N.V. Tarakina, A.P. Tyutyunnik, T.V. D'yachkova, V.G. Zubkov, Yu.G. Zainulin, M. Sayagues, G. Swensson, Zh. Strukt. Khim. 44 (2003) 286 (in Russian); J. Struct. Chem. (Transl. of Zh. Strukt. Khim.) 44 (2003) 252.